

30. Turcotte, D. L. *J. Geophys. Res.* **101**, 4765–4773 (1996).  
 31. Turcotte, D. L. & Schubert, G. *Geodynamics: Applications of Continuum Physics to Geologic Problems* 137–139 Wiley, New York, 1982).  
 32. Solomon, S. C. & Head, J. W. *J. Geophys. Res.* **95**, 11073–11083 (1990).  
 33. Francis, P. W. & Wood, C. A. *J. Geophys. Res.* **87**, 9881–9889 (1982).  
 34. Peale, S. J., Cassen, P. & Reynolds, R. T. *Science* **203**, 892–894 (1979).  
 35. Roy, A. E. *Orbital Motion* 3rd edn 239–279 (Hilger, Philadelphia, 1988).  
 36. Rasio, F. A. & Ford, E. B. *Science* **274**, 954–956 (1996).

**Acknowledgements:** We thank K. Zahnle and R. Lorenz for discussions. D.W. was supported by a NASA graduate student research fellowship (1995); J.K. was supported by the NASA Exobiology Program.

Correspondence and requests for materials should be addressed to D.W. (e-mail: dwilliams@astro.psu.edu).

## Evidence for polaronic supercarriers in the copper oxide superconductors $\text{La}_{2-x}\text{Sr}_x\text{CuO}_4$

Guo-meng Zhao, M. B. Hunt, H. Keller & K. A. Müller

Physik-Institut der Universität Zürich, CH-8057 Zürich, Switzerland

High-temperature superconductivity is known to involve the pairing of charge carriers, but the precise nature of these carriers and the mechanism of their pairing remain unclear. The copper oxides are known to exhibit a strong Jahn–Teller effect — in which spontaneous lattice distortions remove the degeneracy of the electronic ground state — and it has been suggested that the charge carriers are Jahn–Teller polarons (bare charge carriers accompanied by local lattice distortions). In fact, the demonstration<sup>1</sup> that a strong Jahn–Teller effect can lead to the formation of such polarons led to the original discovery of high-temperature superconductivity<sup>2</sup>. Still, direct evidence that Jahn–Teller polarons exist in the superconducting state of the copper oxides has been lacking, although some indirect evidence comes from their recent discovery<sup>3</sup> in the structurally similar but non-superconducting manganite  $\text{La}_{1-x}\text{Ca}_x\text{MnO}_3$ . Here we report the results of magnetization and thermal expansion measurements on samples of the copper oxide superconductor  $\text{La}_{2-x}\text{Sr}_x\text{CuO}_4$  which characterize the oxygen-isotope effects on the carrier density and on the in-plane penetration depth. We find a negligible isotope effect on the former, but a large effect on the latter. Specific quantitative features of the results show that polaronic charge carriers exist and condense into Cooper pairs in the copper oxide superconductors.

Recently there has been increasing evidence that polaronic charge carriers are present in the normal state of the layered copper oxides<sup>4,5</sup>. However, it is not clear whether these normal-state polaronic carriers condense into Cooper pairs. To show that this occurs, it is necessary to demonstrate that the effective supercarrier mass along the  $\text{CuO}_2$  planes ( $m_{ab}^*$ ) depends strongly on ionic mass  $M$  in these layered copper oxide superconductors. In conventional superconductors, only the ‘bare’ carriers condense into the supercarriers, and the supercarrier mass is essentially independent of  $M$ . In the polaronic model<sup>6</sup>, the effective mass of polarons depends strongly on  $M$ . When the polarons condense into supercarriers (by whatever pairing mechanism), the effective supercarrier mass will also depend on  $M$ .

Several groups<sup>7–11</sup> have observed an anomalously large oxygen-isotope effect on the superconducting transition temperature  $T_c$  in underdoped copper oxides, and all of them<sup>8–11</sup> noticed that there is an isotope-dependence of the diamagnetic signal. Zhao *et al.*<sup>12</sup> have studied this effect and tried to interpret it as due to the isotope-mass dependence of the average supercarrier mass  $m^*$  ( $\equiv [(m_{ab}^*)^2 m_c^*]^{1/3}$ ), where  $m_{ab}^*$  and  $m_c^*$  are the effective supercarrier mass along and

perpendicular to the  $\text{CuO}_2$  plane, respectively). However their preliminary data analysis could not determine whether, and how strongly,  $m_{ab}^*$  should depend on the oxygen mass. A quantitative determination of the oxygen-isotope effect on  $m_{ab}^*$  is crucial to the understanding of the physics of high-temperature superconductivity.

Because the magnetic penetration depth  $\lambda(0)$  is proportional to  $\sqrt{m^*/n_s}$ , where  $n_s$  is the supercarrier density, then

$$\Delta m^*/m^* = 2\Delta\lambda(0)/\lambda(0) + \Delta n_s/n_s, \quad (1)$$

where  $\Delta$  means any small change of a quantity upon isotope substitution. Thus the isotope dependence of  $m^*$  can be determined if the isotope dependences of  $\lambda(0)$  and of  $n_s$  can be independently measured.

The isotope dependence of  $\lambda(0)$  can be determined from that of the Meissner fraction  $f(0)$  which, for decoupled and fine-grained samples, depends on the penetration depth  $\lambda(0)$  and on the average grain radius  $R$ , as seen from the Shoenberg formula for spherical grains<sup>13</sup>:

$$f(T) = \frac{3}{2} \left[ 1 - 3 \left( \frac{\lambda(T)}{R} \right) \coth \left( \frac{R}{\lambda(T)} \right) + 3 \left( \frac{\lambda(T)}{R} \right)^2 \right] \quad (2)$$

where  $\lambda(T) = ([(\lambda_{ab}(T))^2 \lambda_c(T)]^{1/3}$  for layered compounds (where  $\lambda_{ab}(T)$  and  $\lambda_c(T)$  are the penetration depths along and perpendicular to the  $\text{CuO}_2$  plane, respectively)<sup>14</sup>. From equation (2), it may be seen that a change in  $\lambda(0)$  will lead to a change in  $f(0)$ , so the isotope dependence of  $\lambda(0)$  can be determined from the isotope dependence of  $f(0)$ .

The isotope dependence of  $n_s$  should be equal to the isotope dependence of the normal carrier density  $n$  in clean superconductors, as is the case in the underdoped copper oxide superconductors<sup>15</sup>. In general, the carrier density  $n$  cannot be measured very precisely by any direct experimental methods, so it is very difficult to determine the isotope dependence of  $n$ . Nevertheless, we note that the structural phase transition temperature  $T_s$  (from the tetragonal to orthorhombic phase) in the  $\text{La}_{2-x}\text{Sr}_x\text{CuO}_4$  system is very sensitive to  $n$ . This implies that a very small difference in  $n$  will lead to a huge difference in  $T_s$ . Thus the isotope dependence of  $n$  can be measured precisely if one can accurately determine the isotope shift of  $T_s$ . It has also been found that there is an anomaly at  $T_s$  in the thermal-expansion coefficient of this system<sup>16,17</sup>. Therefore the isotope shift of  $T_s$  can be precisely determined by a thermal-expansion measurement.

Samples of  $\text{La}_{2-x}\text{Sr}_x\text{CuO}_4$  were prepared by conventional solid-state reaction using  $\text{La}_2\text{O}_3$  (99.99%),  $\text{SrCO}_3$  (99.999%) and  $\text{CuO}$  (99.999%). For the underdoped samples, we used the sample preparation procedures described in ref. 12. To obtain samples with small grains and sufficient porosity for the isotope experiments, we reground the samples thoroughly, pressed them into pellets, and annealed them in air at 900 °C for 12 h. Each pellet was broken in half, and the halves were then subjected to <sup>16</sup>O and <sup>18</sup>O isotope diffusion. The diffusion was carried out for 40 h at 900 °C and oxygen pressure of ~1 bar. The cooling time to room temperature was 4 h. The oxygen isotope enrichment was determined from the weight changes of the <sup>16</sup>O and <sup>18</sup>O samples. The <sup>18</sup>O samples had 85–90% <sup>18</sup>O and ~15–10% <sup>16</sup>O. Back-exchange was carried out at 850 °C for 8 h in air. For the optimally doped samples ( $x = 0.15$ ), the well-mixed powders were calcined for 15 h at 1,000 °C in air. The sintering was performed for 15 h at 1,000 °C in air. Before oxygen isotope diffusion, the samples were ground for about 40 min to ensure that the grain size was as fine as possible. The powder samples were then subject to <sup>16</sup>O and <sup>18</sup>O isotope diffusion at 900 °C for 20 h. The <sup>18</sup>O samples had more than 95% <sup>18</sup>O.

Magnetization was measured with a Quantum Design SQUID magnetometer. The Meissner effect was measured in a magnetic field of 1 mT after the samples had been cooled from the normal state in the field. The magnetic field remained unchanged during

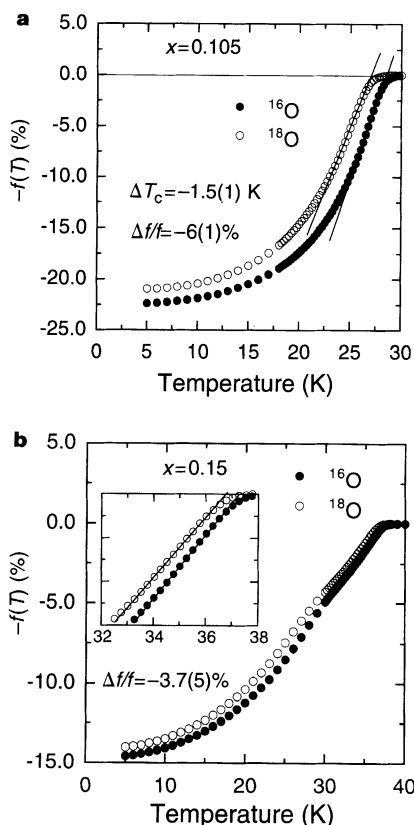


**Figure 1** Temperature dependence of the Meissner effect for  $^{16}\text{O}$  and  $^{18}\text{O}$  samples of  $\text{La}_{2-x}\text{Sr}_x\text{CuO}_4$  with  $x = 0.105$  (a), and  $x = 0.15$  (b). Note that for  $x = 0.15$  there is a small 'bump' in  $f(T)$  due to a change in the effective  $R$  caused by the field-induced decoupling of some weak links.

each series of measurements. For the  $x = 0.15$  samples, we suspended the powders in paraffin to prevent them from moving during magnetization measurements. This technique is essential for the success of this isotope experiment as pelletized samples have too strong intergrain flux trapping at this composition. The thermal expansion was measured on the underdoped samples using a capacitance dilatometer with a length resolution of  $\sim 0.1 \text{ \AA}$ . Data were collected during warming and subsequent cooling at the same constant rate of  $3 \text{ mK s}^{-1}$ .

Figure 1 shows the temperature dependence of the Meissner effect for the  $^{16}\text{O}$  and  $^{18}\text{O}$  samples of  $\text{La}_{2-x}\text{Sr}_x\text{CuO}_4$  with  $x = 0.105$  (Fig. 1a), and  $x = 0.15$  (Fig. 1b). For  $x = 0.105$ , the  $T_c$  of the  $^{18}\text{O}$  sample is lower than that of the  $^{16}\text{O}$  sample by  $\sim 1.5\text{K}$  and the low-temperature Meissner fraction of the  $^{18}\text{O}$  sample is reduced by 6(1)% relative to the  $^{16}\text{O}$  sample (note that 6(1)% means  $6(\pm 1)\%$ ). This is in agreement with the result reported in ref. 12, indicating the excellent reproducibility of these isotope experiments. For the optimally doped samples ( $x = 0.15$ ), the  $T_c$  of the  $^{18}\text{O}$  sample is lower than that of the  $^{16}\text{O}$  sample by  $0.52(4)\text{K}$ , and the low-temperature Meissner fraction of the  $^{18}\text{O}$  sample is reduced by 3.7(5)% relative to the  $^{16}\text{O}$  sample. Both  $T_c$  and the isotope shift are in good agreement with those reported by Franck *et al.*<sup>10</sup>. The broad transition in the  $x = 0.15$  samples is due to a small average grain radius ( $2R \approx 1 \mu\text{m}$ )<sup>9</sup>. We have also shown that there is a small flux trapping in our samples ( $<15\%$  of the Meissner effect), so it will have a negligible effect on the isotope dependence of the Meissner fraction<sup>12</sup>.

It is essential to show that the observed isotope effects are intrinsic. To do this, we took one set of  $^{16}\text{O}$  and  $^{18}\text{O}$  samples of  $\text{La}_{1.895}\text{Sr}_{0.105}\text{CuO}_4$ , and annealed them together in an atmosphere of  $0.2 \text{ bar } ^{16}\text{O}_2$  at  $850^\circ\text{C}$  for 8 h. After annealing, the  $T_c$  and Meissner

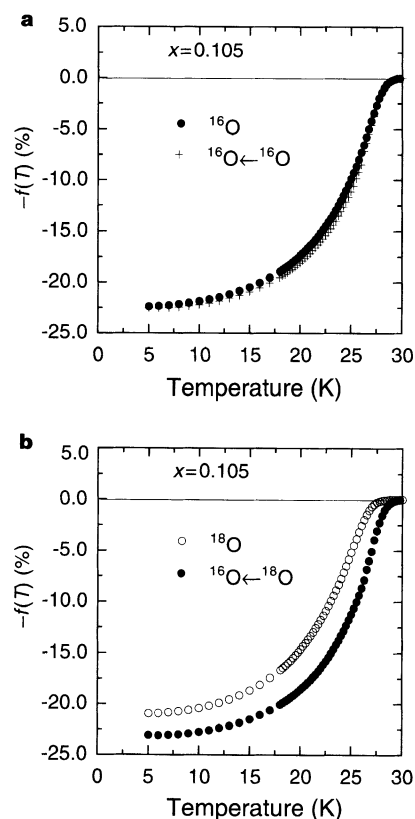


**Figure 2** Temperature dependence of the Meissner effect for one set of  $^{16}\text{O}$  and  $^{18}\text{O}$  samples of  $\text{La}_{1.895}\text{Sr}_{0.105}\text{CuO}_4$  before and after isotope back-exchange: from  $^{18}\text{O}$  to  $^{16}\text{O}$  (a); from  $^{16}\text{O}$  to  $^{18}\text{O}$  (b).

effect for the  $^{16}\text{O}$  sample were nearly unchanged (Fig. 2a). This implies that such a treatment has a negligible effect on the carrier concentration and grain size of the sample. On the other hand, the  $T_c$  and Meissner effect for the  $^{18}\text{O}$  sample changed dramatically (Fig. 2b) due to the back substitution of  $^{16}\text{O}$  for  $^{18}\text{O}$ ; the  $T_c$  of the sample is reduced by  $\sim 1.5\text{K}$ , and the low-temperature Meissner fraction decreases 8(1)%. These results show clearly that the oxygen-isotope substitution indeed leads to substantial reductions in both  $T_c$  and Meissner fraction.

In Fig. 3a we show the linear thermal expansion coefficient  $\beta(T)$  for another set of  $^{16}\text{O}$  and  $^{18}\text{O}$  samples of  $\text{La}_{1.895}\text{Sr}_{0.105}\text{CuO}_4$ , which shows the same oxygen-isotope effects as the set shown in Fig. 1a. There is an anomaly in  $\beta(T)$  at a temperature of  $\sim 265\text{K}$  (marked by an arrow in Fig. 3a), which corresponds to the tetragonal–orthorhombic transition temperature  $T_s$  (ref. 17). It is clear that the two curves nearly overlap, implying that the two isotope samples have the same  $T_s$  within the uncertainty of our measurements ( $\leq 0.3\text{K}$ ). In Fig. 3b we show the dependence of  $T_s$  on the Sr content  $x$ , as determined by further thermal expansion measurements. A linear fit to the data with  $T_s = A - Bx$  gives  $A = 569\text{K}$  and  $B = 2,900\text{K}$ . This relation implies that  $T_s = 569\text{K}$  for  $x = 0$ , and  $T_s = 0$  for  $x = 0.20$ , which is in fair agreement with reported results<sup>18,19</sup>. It has also been shown by Dabrowski *et al.*<sup>19</sup> that  $T_s$  is mainly determined by the hole concentration, although the mean ionic radius at the cation site has a small effect on  $T_s$  (for example, the composition  $x_c$  at which  $T_s = 0$  is  $\sim 0.2$  in  $\text{La}_{2-x}\text{Sr}_x\text{CuO}_4$ , and  $\sim 0.25$  in  $\text{La}_{2-x}\text{Ca}_x\text{CuO}_4$ ). Then, with  $n = x$ , we can write  $dT_s/dn \approx dT_s/dx = B$ . Using  $\Delta T_s \leq 0.3\text{K}$  and  $n = 0.105$ , we obtain  $|\Delta n/n| = |(1/nB)\Delta T_s| \leq 0.1\%$ . Thus, there is a negligible oxygen-isotope effect on  $n$ . In addition, we have shown that the ratio of the normal-state susceptibilities (including a small Curie

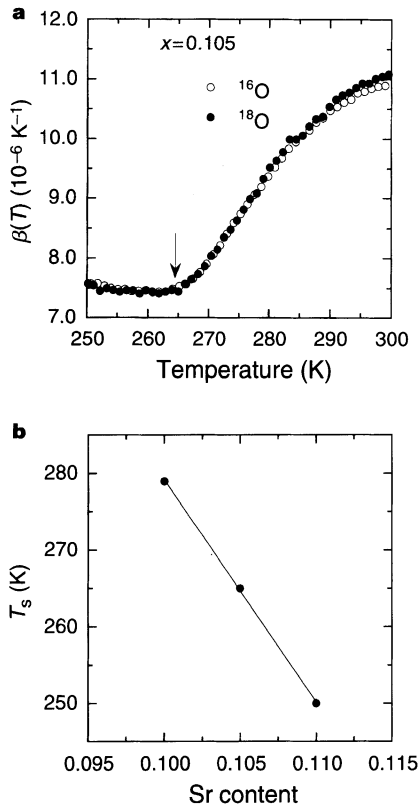


**Figure 3** The linear thermal expansion coefficient  $\beta(T)$  for the  $^{16}\text{O}$  and  $^{18}\text{O}$  samples of  $\text{La}_{1.895}\text{Sr}_{0.105}\text{CuO}_4$  (**a**), and the dependence of the tetragonal-orthorhombic transition temperature  $T_s$  on the Sr content  $x$  (**b**).

term contributed by some localized carriers) for the two isotope samples is temperature-independent down to a temperature near  $T_c$ . This implies that the two isotope samples must have the same mobile carrier concentration near  $T_c$  even if charge localization occurs. Fiory *et al.*<sup>20</sup> have shown that the carrier concentration in slightly underdoped  $\text{YBa}_2\text{Cu}_3\text{O}_{7-y}$  is nearly the same in the normal and superconducting states, as expected for a clean superconductor. We would expect the same result in the clean one-layer superconductor  $\text{La}_{2-x}\text{Sr}_x\text{CuO}_4$ . Thus our results imply that there is a negligible oxygen-isotope effect on the supercarrier density  $n_s$ .

We now consider the determination of the oxygen-mass dependence of the penetration depth from equation (2) and the measured oxygen-isotope effect on  $f(0)$ . From equation (2), we obtain

$$\Delta\lambda(0)/\lambda(0) = C(R)\Delta f(0)/f(0) \quad (3)$$

where  $C(R) = [f(0)/\lambda(0)](\partial\lambda/\partial f)$ , which implicitly depends on  $f(0)$  (for example, for  $f(0) = 22\%$ ,  $C(R) = -0.63$ ;  $f(0) = 14\%$ ,  $C(R) = -0.57$ ). From equation (3), and using measured values of  $f(0) = 22\%$  and  $\Delta f(0)/f(0) = -6(1)\%$  for  $x = 0.105$ , we find  $\Delta\lambda(0)/\lambda(0) = 3.8(5)\%$ . Similarly, for  $x = 0.15$ , using  $f(0) = 14\%$  and  $\Delta f(0)/f(0) = 3.7(5)\%$ , we find  $\Delta\lambda(0)/\lambda(0) = 2.1(3)\%$ . Shibauchi *et al.*<sup>21</sup> showed that, due to the intrinsic Josephson coupling between the  $\text{CuO}_2$  planes, the penetration depth along the  $c$ -direction  $\lambda_c(0) \propto \sqrt{(\rho_c/T_c)}$  in  $\text{La}_{2-x}\text{Sr}_x\text{CuO}_4$ , where  $\rho_c$  is the resistivity along the  $c$ -direction. The resistivity is independent of the isotope mass in the case of the polaronic hopping conductivity observed in this system<sup>5</sup>. Using  $\lambda(0) = ((\lambda_{ab}(0))^2\lambda_c(0))^{1/3}$  we find

$$\Delta\lambda_{ab}(0)/\lambda_{ab}(0) = \frac{3}{2} [\Delta\lambda(0)/\lambda(0)] + \frac{1}{4} (\Delta T_c/T_c) \quad (4)$$

Substituting  $\Delta\lambda(0)/\lambda(0) = 3.8(5)\%$  and  $\Delta T_c/T_c = -5.4(4)\%$  for  $x = 0.105$ , into equation (4), we get  $\Delta\lambda_{ab}(0)/\lambda_{ab}(0) = 4.4(5)\%$ .

Then  $\Delta m_{ab}^*/m_{ab}^* = 2\Delta\lambda_{ab}(0)/\lambda_{ab}(0) = 9(1)\%$  given that  $\Delta n_s/n_s = 0$ . If we define the exponent of the oxygen-isotope effect on  $m_{ab}^*$  as  $\alpha_{m^*}^o = -\text{dln}m_{ab}^*/\text{dln}M_o$ , then  $\alpha_{m^*}^o = -0.8(1)$  for  $x = 0.105$ . In the same way, we obtain  $\Delta m_{ab}^*/m_{ab}^* = 5.6(5)\%$  and  $\alpha_{m^*}^o = 0.46(5)$  for  $x = 0.15$ .

We now discuss the isotope dependence of  $m_{ab}^*$  on the basis of the polaron model<sup>6</sup>. In this model, the effective mass of polarons ( $m_{ab}^p$ ) is given as

$$m_{ab}^p \propto \exp(\gamma E_b/\hbar\omega) \quad (5)$$

where  $E_b$  is the binding energy of polarons, and is independent of the isotope mass,  $\gamma$  is a dimensionless constant ( $0 \leq \gamma \leq 1$ ) which increases with increasing  $E_b/t$  (where  $t$  is the bare hopping integral) and  $\omega$  is the characteristic frequency of the optical phonons. From equation (5), the total exponent of the isotope effect on  $m_{ab}^p$  is

$$\alpha_{m^p}^i = -\text{dln}m_{ab}^p/\text{dln}M_o = -0.5\gamma E_b/\hbar\omega \quad (6)$$

Furthermore, if we assume that the polaronic carriers condense into Cooper pairs, then  $m_{ab}^* = m_{ab}^p(1 + \lambda_{cb})$ , where the coupling constant  $\lambda_{cb} = N^p(0)V$  with  $N^p(0)$  being the density of states of the polaronic conduction band ( $\propto m_{ab}^p$ ) and  $V$  being the pairing potential which could arise from phonons and/or other bosonic excitations. It is well established that the coupling in the hole-doped cuprates is very strong ( $\lambda_{cb} \geq 3$ ), as seen from the large reduced gap ( $2\Delta_{\text{max}}/k_B T_c = 8$ ) measured for optimally doped  $\text{YBa}_2\text{Cu}_3\text{O}_7$ ,  $\text{Bi}_2\text{Sr}_2\text{CaCu}_2\text{O}_8$  and  $\text{La}_{1.83}\text{Sr}_{0.17}\text{CuO}_4$  compounds<sup>22,23</sup>. For  $\lambda_{cb} \gg 1$ ,  $m_{ab}^* \propto (m_{ab}^p)^2$  so that  $\Delta m_{ab}^p/m_{ab}^p \approx \frac{1}{2}\Delta m_{ab}^*/m_{ab}^*$ , or  $\alpha_{m^p}^i = \frac{1}{2}\alpha_{m^*}^i$ . Moreover, one would expect that  $\alpha_{m^*}^i = 2\alpha_{m^p}^i$  because the oxygen- and copper-isotope effects on  $T_c$  have the same exponent in underdoped  $\text{La}_{2-x}\text{Sr}_x\text{CuO}_4$  (ref. 10), and because there should be no contribution to the isotope effect from La and Sr atoms. Then we have  $\alpha_{m^p}^i = \alpha_{m^*}^o$ , leading to

$$\alpha_{m^*}^o = -0.5\gamma E_b/\hbar\omega \quad (7)$$

From equations (5) and (7), we find that the effective mass of polarons is enhanced by a factor  $\exp(\gamma E_b/\hbar\omega) = \exp(-2\alpha_{m^*}^o)$  with respect to the bare mass. For  $x = 0.105$ , this enhancement factor is intermediate ( $\sim 5.0$ ), and decreases further towards the optimally doped regime ( $\sim 2.5$ ). As the coupling constant should be nearly doping-independent owing to the doping-independence of the superconducting gap<sup>24,25</sup>, the supercarrier mass  $m_{ab}^*$  for the optimally-doped sample will be about half that for the  $x = 0.105$  sample. This implies that  $m_{ab}^*/n_s$  for the optimally-doped sample is about one-third that for the  $x = 0.105$  sample (because  $n_s$  for  $x = 0.15$  is  $\sim 1.5$  times larger than that for  $x = 0.105$ ), in excellent agreement with the muon spin rotation measurement<sup>10</sup>. Moreover, from equation (7) and the measured values of  $\alpha_{m^*}^o$  for  $x = 0.105$  and  $0.15$ , we see the polaron binding energy  $E_b$  for  $x = 0.15$  is about half that for  $x = 0.105$ , in fair agreement with the optical measurements in this system ( $E_b = 0.12$  eV for  $x = 0.10$ , and  $E_b = 0.06$  eV for  $x = 0.15$ )<sup>5</sup>. The above consistency leads us to conclude that polaronic charge carriers exist and condense into Cooper pairs in high-temperature superconductors. The mechanism for the formation of polarons may arise from a strong Jahn-Teller effect, as is the case in manganites<sup>3</sup>, which would be consistent with the theory proposed by Höck *et al.*<sup>1</sup> □

Received 19 August; accepted 20 November 1996.

- Höck, K.-H., Nickisch, H. & Thomas, H. *Helv. Phys. Acta* **56**, 237–243 (1983).
- Bednorz, J. G. & Müller, K. A. *Z. Phys. B* **64**, 189–193 (1986).
- Zho, G. M., Conder, K., Keller, H. & Müller, K. A. *Nature* **381**, 676–678 (1996).
- Proc. Int. Workshop on Anharmonic Properties of High- $T_c$  Cuprates* (eds Mihailowic, D., Ruani, G., Kaldis, E. & Müller, K. A.) 118–146 (World Scientific, Singapore, 1994).
- Bi, X. X. & Eklund, P. C. *Phys. Rev. Lett.* **70**, 2625–2628 (1993).
- Alexandrov, A. S. & Mott, N. F. *Int. J. Mod. Phys. B*, 2075–2109 (1994).
- Crawford, M. K., Kunchur, M. N., Farneth, W. E., McCarron, E. M. & Poon, S. J. *Phys. Rev. B* **41**, 282–287 (1990).
- Crawford, M. K., Farneth, W. E., McCarron, E. M., Harlow, R. L. & Moudren, A. H. *Science* **250**, 1390–1394 (1990).
- Ronay, M., Frisch, M. A. & McGuire, T. R. *Phys. Rev. B* **45**, 355–360 (1992).
- Franck, J. P., Harker, S. & Brewer, J. H. *Phys. Rev. Lett.* **71**, 283–286 (1993).

11. Bornemann, H. J. & Morris, D. E. *Phys. Rev. B* **44**, 5322–5325 (1991).
12. Zhao, G. M., Singh, K. K., Sinha, A. P. B. & Morris, D. E. *Phys. Rev. B* **52**, 6840–6844 (1995).
13. Shoenberg, D. *Proc. R. Soc. Lond. A* **175**, 49–70 (1940).
14. Kogan, V. G., Fang, M. M. & Mitra, S. *Phys. Rev. B* **38**, 11958–11961 (1988).
15. Uemura, Y. J. *et al. Phys. Rev. Lett.* **62**, 2317–2320 (1989).
16. Sarrao, J. L. *et al. Phys. Rev. B* **50**, 13125–13131 (1994).
17. Okajima, Y., Hashimoto, S. & Yamaya, K. *Physica C* **235–240**, 1317–1318 (1994).
18. Kato, M., Maeno, Y. & Fujita, T. *Physica C* **152**, 116–120 (1988).
19. Dabrowski, B. *et al. Phys. Rev. Lett.* **76**, 1348–1351 (1996).
20. Fiory, A. T. *et al. Phys. Rev. Lett.* **65**, 3441–3444 (1990).
21. Shibauchi, T. *et al. Phys. Rev. Lett.* **72**, 2263–2266 (1994).
22. Ekino, T. M., Fujii, H. & Akimitsu, J. *Physica C* **235–240**, 1899–1900 (1994).
23. Chen, X. K., Irwin, J. C., Trodahl, H. J., Kimura, T. & Kishio, K. *Phys. Rev. Lett.* **73**, 3290–3293 (1994).
24. Ding, H. *et al. Nature* **382**, 51–54 (1996).
25. Loram, J. W., Mirza, K. A., Wade, J. M., Cooper, J. R. & Liang, W. Y. *Physica C* **235–240**, 134–137 (1994).

**Acknowledgements:** We thank W. Paul for use of the dilatometer at the ABB Research Center. This work was supported by the Swiss National Science Foundation.

Correspondence and requests for materials should be addressed to H.K. (e-mail: keller@physik-zru.unizh.ch).

## Conversion of light energy to proton potential in liposomes by artificial photosynthetic reaction centres

Gali Steinberg-Yfrach, Paul A. Liddell, Su-Chun Hung, Ana L. Moore, Devens Gust & Thomas A. Moore

Center for The Study of Early Events in Photosynthesis and Department of Chemistry & Biochemistry, Arizona State University, Tempe, Arizona 85287-1604, USA

During photosynthesis, photoinduced electron transport across membranes is carried out by pigment molecules organized into reaction centres by membrane-spanning proteins. The resulting transmembrane electrochemical potential is then coupled to the movement of protons across the membrane<sup>1</sup>. Photoinduced electron transport followed by thermal electron transfer, leading to charge separation over distances of 8 nm, has been demonstrated in artificial mimics of the photosynthetic reaction centre comprising covalently linked electron donors and acceptors<sup>2–10</sup>. Here we report the assembly of an artificial mimic of the photosynthetic apparatus which transports protons across a lipid bilayer when illuminated. Our model reaction centre is a molecular ‘triad’, consisting of an electron donor and acceptor linked to a photosensitive porphyrin group. This triad is incorporated into the bilayer of a liposome. When excited, it establishes a reduction potential near the outer surface of the bilayer and an oxidation potential near its inner surface. In response to this redox potential gradient, a freely diffusing quinone molecule alternates between its oxidized and reduced forms to ferry protons across the bilayer with an overall quantum yield of 0.004, creating a pH gradient between the inside and outside of the liposome.

Molecular triad **1** (Fig. 1 bottom) was prepared by linking a synthetic tetraarylporphyrin (P) to both a naphthoquinone moiety fused to a norbornene system bearing a carboxylic acid group (Q) and a carotenoid polyene (C)<sup>11</sup>. On excitation, the triad (dissolved in various solvents) undergoes photoinduced electron transfer from the excited singlet state of the porphyrin moiety to yield the intermediate charge-separated species C–P<sup>+</sup>–Q<sup>–</sup> with a quantum yield of ~1. Subsequent electron transfer from the carotenoid to the porphyrin radical cation competes with charge recombination to give C<sup>+</sup>–P–Q<sup>–</sup> with a quantum yield up to 0.15 (ref. 11).

Liposomes were prepared by standard reverse-phase evaporation

procedures<sup>12</sup> from a lipid mixture that contained the lipid-soluble 2,5-diphenylbenzoquinone (Q<sub>s</sub>; Fig. 1 bottom) as the proton shuttle. Vectorial electron and proton transport requires asymmetric insertion of the molecular triad artificial reaction centre into the liposomal bilayer membrane. This was accomplished by injection of a tetrahydrofuran solution of **1** into an aqueous solution containing liposomes, a procedure which delivers **1** to the outside surface of the bilayer. A preference for the directional order indicated in Fig. 1 (top) is expected because insertion of the lipophilic carotenoid of **1** into the bilayer avoids the energetic cost of moving the polar, carboxylate-bearing quinone through the low-dielectric medium.

Laser flash photolysis experiments on liposomes containing **1** are

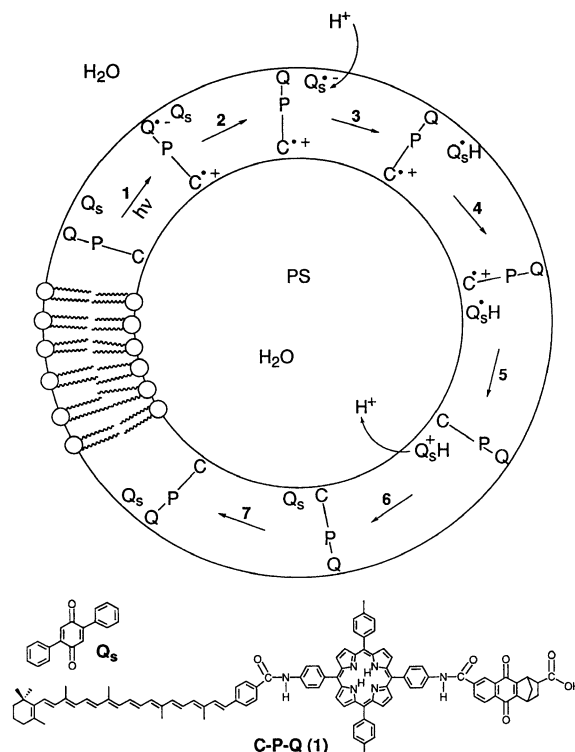


**Figure 1** Bottom, Structures of triad **1** and 2,5-diphenylbenzoquinone (Q<sub>s</sub>); top, schematic diagram illustrating the orientation of triad **1** in a liposome, with its quinone near the interface between the bulk aqueous phase and the bilayer lipid membrane. Steps 1–7 illustrate the proposed elementary processes involved in proton translocation across the liposomal bilayer. Reverse-phase evaporation (RPE) liposomes were prepared by standard procedures using 5 mg of a 2:3 molar ratio of L- $\alpha$ -phosphatidylserine (brain, ~60% 1-stearoyl-2-oleoylphosphatidylserine) and dioleoylphosphatidylcholine<sup>12</sup>. The solution also contained 0.05 M KCl and pyraninetrisulphonate (PS), a water-soluble dye which indicates the pH by the ratio of the amplitude of the fluorescence excitation spectrum at 406 nm to that at 456 nm ( $I_{406}/I_{456}$ ) (ref. 18). For certain experiments, the lipid mixture also contained 0.4 mg of lipid-soluble Q<sub>s</sub> as the proton shuttle. The midpoint potential for the one-electron reduction of Q<sub>s</sub> is more positive by ~0.6 V than that of the quinone component of **1** (ref. 19). Triad **1** was added to a stirred solution of liposomes by injection of 30–40  $\mu$ l of a  $7.7 \times 10^{-5}$  M solution of **1** in tetrahydrofuran. The liposomes were then purified by gel chromatography (Sephadex G-100; elution with a 0.05 M KCl solution). Quantitative analysis<sup>20</sup> of the organic phosphorus in these liposomes indicated that they typically contain  $\sim 5 \times 10^{17}$  molecules of lipid per ml. RPE liposomes formed in this way have  $\sim 8 \times 10^4$  molecules lipid per liposome (therefore,  $\sim 5 \times 10^{12}$  liposomes per ml), an average diameter of 100 nm and an average volume of  $5 \times 10^{-18}$  l (ref. 12). Based on the amount of dye and **1** extracted from a typical liposome preparation, there are ~40 molecules of **1** in the bilayer and ~50 molecules of PS in the interior aqueous phase of each liposome.